JOURNAL OF MOLECULAR SPECTROSCOPY 5, 390–404 (1960)

Vibration-Rotation Energies of Tetrahedral XY_4 Molecules

Part II. The Fundamental ν_3 of CH_4*

KARL T. HECHT

The Harrison M. Randall Laboratory of Physics, The University of Michigan, Ann Arbor, Michigan

The matrix elements derived in the first paper of this series are used to compute the frequencies of the tetrahedral fine structure components of the rotational lines of the fundamental ν_3 of CH_4. The theoretically predicted frequencies are compared with the recent high resolution spectra of Plyler *et al.* A best fit for the splitting patterns is obtained with the following splitting constants: $t_{224} = -2.93 \times 10^{-3}$ cm^{-1}, $t_{134} = 0$, $t_{044} = -4.5 \times 10^{-6}$ cm^{-1}, $t_{244} = -5.0 \times 10^{-6}$ cm^{-1}. Analysis of the unperturbed frequency positions and the weak forbidden P and R branch lines gives the following rotational constants: $B_0 = 5.240$ cm^{-1}, $D_s = 1.0 \times 10^{-4}$ cm^{-1}, $B_3(R = J) = 5.191$ cm^{-1}, $B_3(R = J + 1, J - 1) = 5.201$ cm^{-1}, $\zeta_3 = 0.054_7$.

INTRODUCTION

In the first paper of this series (*1*) the theory of the vibration-rotation perturbations in tetrahedral XY_4 molecules was re-examined in terms of the modern theory of angular momentum coupling. It was shown that the splitting of a vibration-rotation level into its tetrahedral sublevels is governed by perturbation terms of one basic symmetry in all states in which only quanta of ν_1, ν_3, and ν_4 are excited. As a result all such bands show the same basic splitting patterns. In dominant approximation the relative spacings of the A_1, A_2, E, F_1, and F_2 fine structure levels of a state of given rotational angular momentum are the same in all infrared active bands and can therefore be obtained from the results of Jahn (*2*) for the fundamental ν_4. Only the overall separation of the fine structure lines will vary from band to band. In next approximation, however, the basic splitting patterns are deformed by matrix elements off-diagonal in the rotational angular momentum quantum number R, and this effect becomes important in trying to account for the modern high resolution spectra. From the matrix elements tabulated in (*1*) both the basic splitting patterns and the extent to which they are deformed may be calculated. In this paper the results of such calculations for the fundamental ν_3 of CH_4 will be presented and compared with the recent high resolution spectra of Plyler *et al.* (*3*).

* This work has been supported in part by the Office of Naval Research under Navy Theoretical Physics Contract No. Nonr 1224(15).

GROUND STATE ENERGIES

It was shown in (*1*) that the splitting of the rotational levels of the vibrational ground state into their tetrahedral sublevels is given by a single perturbation term and increases with an approximate J^4 dependence. The magnitude of the splitting is determined by the coefficient.

$$D_t = \frac{B^3}{5}\left[\frac{1}{\omega_2^2} - \frac{\zeta_{23}^2}{\omega_3^2} - \frac{\zeta_{24}^2}{\omega_4^2}\right]. \tag{1}$$

The splitting perturbations for $J \leqq 8$ are given in terms of D_t in Table I. Although the ground state splittings are negligible for very low J values, the numbers in Table I are significant since the *relative* spacings of the tetrahedral sublevels of a state of given rotational angular momentum, R, are, in dominant approximation, basic to almost all vibrational levels. (In the ground state $R = J$). For values of $J > 8$ some of the splitting perturbations involve the roots of cubic and higher degree equations and are therefore best tabulated numerically. Numerical values of the ground state splitting perturbations are given in Table II for which a best value of D_t of 4.5×10^{-6} cm^{-1} has been used. From the known values of B, the zetas, and the most recent estimates of Jones and McDowell (*4*) for the ω_i, Eq. (1) yields a value of D_t of 4.0×10^{-6} cm^{-1}.

TABLE I

GROUND-STATE SPLITTING PERTURBATIONS: BASIC PATTERNS $J = 0$ TO 8

$J = 0$	A_1	0	$J = 6$	A_1	$63 \cdot 60D_t$
				F_1	$48 \cdot 60D_t$
$J = 1$	F_2	0		F_2	$(-10 + 2\sqrt{421}) \cdot 60D_t$
				A_2	$-33 \cdot 60D_t$
$J = 2$	F_2	$2 \cdot 12D_t$		F_2	$(-10 - 2\sqrt{421}) \cdot 60D_t$
	E	$-3 \cdot 12D_t$		E	$-57 \cdot 60D_t$
$J = 3$	A_1	$6 \cdot 60D_t$	$J = 7$	F_2	$(-13 + 20\sqrt{694}) \cdot 12D_t$
	F_1	$1 \cdot 60D_t$		E	$352 \cdot 12D_t$
	F_2	$-3 \cdot 60D_t$		F_1	$247 \cdot 12D_t$
				A_1	$52 \cdot 12D_t$
$J = 4$	F_2	$13 \cdot 60D_t$		F_1	$-473 \cdot 12D_t$
	E	$-2 \cdot 60D_t$		F_2	$(-13 - 20\sqrt{694}) \cdot 12D_t$
	F_1	$-7 \cdot 60D_t$			
	A_1	$-14 \cdot 60D_t$	$J = 8$	F_2	$(91 + 8\sqrt{91}) \cdot 60D_t$
				E	$14(-1 + \sqrt{943/7}) \cdot 60D_t$
$J = 5$	F_2	$6\sqrt{21} \cdot 60D_t$		F_1	$(-49 + 36\sqrt{14}) \cdot 60D_t$
	E	$21 \cdot 60D_t$		F_2	$(91 - 8\sqrt{91}) \cdot 60D_t$
	F_1	$-14 \cdot 60D_t$		E	$14(-1 - \sqrt{943/7}) \cdot 60D_t$
	F_2	$-6\sqrt{21} \cdot 60D_t$		F_1	$(-49 - 36\sqrt{14}) \cdot 60D_t$
				A_1	$-196 \cdot 60D_t$

TABLE II

GROUND-STATE SPLITTING PERTURBATIONS: NUMERICAL VALUES

	J = 13		*J* = 11		*J* = 9
$F_2^{(4)}$	0.302 cm^{-1}	$F_2^{(3)}$	0.156 cm^{-1}	A_1	0.075 cm^{-1}
$E^{(2)}$	0.283	$E^{(2)}$	0.146	$F_1^{(2)}$	0.067
$F_1^{(3)}$	0.265	$F_1^{(3)}$	0.124	$F_2^{(3)}$	0.057
A_1	0.162	$F_2^{(2)}$	0.062	A_2	0.032
$F_1^{(2)}$	0.111	$E^{(1)}$	−0.012	$F_2^{(2)}$	0.006
$F_2^{(3)}$	0.079	$F_1^{(2)}$	−0.021	E	0.000
A_2	−0.080	A_1	−0.036	$F_1^{(1)}$	−0.081
$F_2^{(2)}$	−0.097	$F_1^{(1)}$	−0.197	$F_2^{(1)}$	−0.085
$E^{(1)}$	−0.104	$F_2^{(1)}$	−0.199		*J* = 8
$F_1^{(1)}$	−0.403		*J* = 10	$F_2^{(2)}$	0.045 cm^{-1}
$F_2^{(1)}$	−0.406	$F_2^{(3)}$	0.108 cm^{-1}	$E^{(2)}$	0.040
	J = 12	$E^{(2)}$	0.094	$F_1^{(2)}$	0.024
$A_1^{(2)}$	0.226 cm^{-1}	$F_1^{(2)}$	0.082	$F_2^{(1)}$	0.005
$F_1^{(3)}$	0.214	A_1	0.045	$E^{(1)}$	−0.048
$F_2^{(3)}$	0.197	$F_1^{(1)}$	0.004	$F_1^{(1)}$	−0.050
A_2	0.169	$F_2^{(2)}$	−0.010	A_1	−0.053
$E^{(2)}$	0.090	A_2	−0.128		*J* = 7
$F_2^{(2)}$	0.089	$F_2^{(1)}$	−0.130	$F_2^{(2)}$	0.028 cm^{-1}
$F_1^{(2)}$	−0.042	$E^{(1)}$	−0.133	E	0.019
$F_2^{(1)}$	−0.060		*J* = 6	$F_1^{(2)}$	0.013
$F_1^{(1)}$	−0.287	A_1	0.017 cm^{-1}	A_1	0.003
$A_1^{(1)}$	−0.289	F_1	0.013	$F_1^{(1)}$	−0.026
$E^{(1)}$	−0.304	$F_2^{(2)}$	0.008	$F_2^{(1)}$	−0.029
	J ≦ 5	A_2	−0.009		
All	<0.01	$F_2^{(1)}$	−0.014		
		E	−0.015		

EXCITED STATE ENERGIES

It was shown in (*1*) that the splitting of the energy levels of the excited state of the fundamental ν_3 are to third order of approximation determined by three perturbation terms. All of them involve the same basic linear combination of fourth rank tensor operators but differ in their J-dependence, increasing approximately with J^2, J^3, and J^4. The coefficients of these terms were denoted by t_{224}, t_{134}, and t_{044}, respectively, where the subscripts i, j, k of t_{ijk} indicate the tensor character of the terms. The overall rank of the perturbation operators is indicated by k ($= 4$), while the rank of the vibrational and rotational operators from which the vibration-rotation perturbation terms are built is indicated by i and j, respectively. In order to fit accurately all the observed P, Q, and R branch lines of the fundamental ν_3 it was found necessary to add a fourth term, of type t_{244}. Formally such a term would appear only in the fourth-order Hamiltonian. Since it is a perturbation term of the same fourth-rank tensor character as the second- and third-order perturbation terms, however, its effect can easily

be included with the previous calculations. An operator of this type merely adds an additional coefficient with an approximate J^4 dependence. Its effect can be included if the quantities $f_{044}t_{044}$ of (*1*) are augmented by a new term $f_{244}t_{244}$. The quantities $f_{044}t_{044} + f_{244}t_{244}$ are listed below for the various possible values of R and R' of the excited state: For

$$\begin{aligned}
&R' = (J+1) \quad R = (J+1) \quad \tfrac{1}{2}(2J^2 - 5J + 3)(t_{044} + t_{244}),\\
&R' = J \quad\quad R = J \quad\quad (J^2 + J - 10)t_{044} - 2(J^2 + J + 5)t_{244},\\
&R' = (J-1) \quad R = (J-1) \quad \tfrac{1}{2}(2J^2 + 9J + 10)(t_{044} + t_{244}),\\
&R' = J \quad\quad R = (J+1) \quad (2J - 3)[t_{044} - \tfrac{1}{20}(3J - 17)t_{244}],\\
&R' = (J-1) \quad R = (J+1) \quad 3[t_{044} - \tfrac{1}{60}(36J^2 + 36J - 51)t_{244}],\\
&R' = (J-1) \quad R = J \quad\quad (2J + 5)[t_{044} + \tfrac{1}{20}(3J + 20)t_{244}].
\end{aligned} \tag{2}$$

It is to be noted that a tensor operator of type 244 can not contribute to the ground state energies.

In dominant approximation the relative separations of the tetrahedral sublevels of a state of given rotational angular momentum are given by the ratios of Table I. In next approximation, however, these splitting patterns are deformed by the matrix elements off-diagonal in the quantum number R. In order to fit accurately the high resolution spectra of Plyler *et al.* (*3*) it is necessary to include the contributions of such matrix elements. For this reason the complete Hamiltonian matrices for specific values of J and tetrahedral symmetry have been diagonalized using the matrix elements of (*1*) and several trial values for the coefficients t_{ijk}.[1] The best fit between theory and experiment was obtained with the following values for the coefficients:

$$\begin{aligned}
t_{224} &= -2.93 \times 10^{-3}\ \text{cm}^{-1},\\
t_{134} &= 0,\\
t_{044} &= -4.5 \times 10^{-6}\ \text{cm}^{-1},\\
t_{244} &= -5.0 \times 10^{-6}\ \text{cm}^{-1}.
\end{aligned}$$

(To third order $t_{044} = -D_t$, t_{224} is given in terms of the molecular parameters in the previous paper (*1*).) The dominant contribution is given by the coefficient t_{224}, but the contributions of t_{044} and t_{244} become important for large values of J. The results of the diagonalization are shown in Tables III–V, which give the splitting perturbations for the states J_{J+1}, J_J, and J_{J-1}, respectively. For

[1] The diagonalization was carried out with an IBM 650 computing machine and was checked with a perturbation technique. It was seen in (*1*) that the diagonalization involves a 3×3 matrix for states $3\,F_2$. The largest matrix encountered was a 10×10 matrix for states $12\,F_2$.

TABLE III

J_{J+1} LEVELS: SPLITTING PERTURBATIONS

0_1	F_2	0	7_8	A_1	0.531 cm^{-1}	10_{11}	$E^{(1)}$	0.355 cm^{-1}
1_2	E	0.035 cm^{-1}		$F_1^{(1)}$	0.497		A_1	0.287
	F_2	−0.023		$E^{(1)}$	0.474		$F_2^{(2)}$	0.148
2_3	F_2	0.070		$F_2^{(1)}$	0.121		$F_1^{(3)}$	−0.280
	F_1	0.023		$F_1^{(2)}$	−0.173		$E^{(2)}$	−0.400
	A_1	−0.140		$E^{(2)}$	−0.294		$F_2^{(3)}$	−0.454
3_4	A_1	0.174		$F_2^{(2)}$	−0.355	11_{12}	$A_1^{(1)}$	0.988
	F_1	0.092	8_9	$F_2^{(1)}$	0.651		$F_1^{(1)}$	0.975
	E	0.028		$F_1^{(1)}$	0.606		$E^{(1)}$	0.937
	F_2	−0.149		E	0.207		$F_2^{(1)}$	0.610
4_5	$F_2^{(1)}$	0.223		$F_2^{(2)}$	0.155		$F_1^{(2)}$	0.481
	F_1	0.111		A_2	−0.126		$E^{(2)}$	0.297
	E	−0.124		$F_2^{(3)}$	−0.322		$F_2^{(2)}$	0.240
	$F_2^{(2)}$	−0.194		$F_1^{(2)}$	−0.365		A_2	−0.315
5_6	E	0.301		A_1	−0.437		$F_2^{(3)}$	−0.372
	$F_2^{(1)}$	0.273	9_{10}	$E^{(1)}$	0.759		$F_1^{(3)}$	−0.397
	A_2	0.168		$F_2^{(1)}$	0.748		$A_1^{(2)}$	−0.436
	$F_2^{(2)}$	−0.102		A_2	0.722	12_{13}	$F_2^{(1)}$	1.072
	F_1	−0.202		$F_2^{(2)}$	0.316		$F_1^{(1)}$	1.046
	A_1	−0.293		$F_1^{(1)}$	0.234		$E^{(1)}$	0.762
6_7	$F_2^{(1)}$	0.400		A_1	0.069		$F_2^{(2)}$	0.720
	$F_1^{(1)}$	0.351		$F_1^{(2)}$	−0.262		A_2	0.576
	A_1	0.082		$E^{(2)}$	−0.339		$F_2^{(3)}$	0.433
	$F_1^{(2)}$	−0.098		$F_2^{(3)}$	−0.432		$F_1^{(2)}$	0.369
	E	−0.189	10_{11}	$F_2^{(1)}$	0.877		A_1	0.046
	$F_2^{(2)}$	−0.315		$F_1^{(1)}$	0.870		$F_1^{(3)}$	−0.329
				$F_1^{(2)}$	0.388		$F_2^{(4)}$	−0.371
							$E^{(2)}$	−0.426

small values of the angular momentum quantum numbers the relative separations of the tetrahedral sublevels are approximated rather well by the basic splitting ratios of Table I. For larger values of R, however, the effect of the off-diagonal matrix elements becomes important. For example, the A_1, $F_1^{(1)}$, $E^{(1)}$, $F_2^{(1)}$, $F_1^{(2)}$, $E^{(2)}$, and $F_2^{(2)}$ states of 7_8 are predicted to be spilt from their unperturbed position in the ratios (196), 183.4, 175.0, 44.6, −63.9, −108.5, and −131.0, respectively (Table III). The corresponding splitting ratios would have been (196), 183.7, 176.5, −14.7, −85.7, −148.5, and −167.3 if matrix elements off-diagonal in R had been neglected (Table I).

COMPARISON BETWEEN THEORY AND EXPERIMENT

The comparison between theory and experiment is made in Table VI for the P-branch lines. The first column gives the observed frequencies of Plyler *et al.* (*3*). The second column shows the unperturbed frequencies after the correction for the splitting perturbations has been made. For example, the A_1 line of $P(8)$

TABLE IV

J_J LEVELS: SPLITTING PERTURBATIONS

1_1	F_1	0	8_8	$F_1^{(2)}$	0.750 cm^{-1}	11_{11}	$F_1^{(3)}$	1.298 cm^{-1}
2_2	F_1	0.023 cm^{-1}		$E^{(2)}$	0.652		$E^{(2)}$	1.219
	E	−0.035		$F_2^{(2)}$	0.336		$F_2^{(3)}$	0.982
3_3	A_2	0.171		$F_1^{(1)}$	0.077		$F_1^{(2)}$	0.657
	F_2	0.017		$E^{(1)}$	−0.917		$E^{(1)}$	−0.044
	F_1	−0.091		$F_2^{(1)}$	−0.959		$F_2^{(2)}$	−0.082
4_4	F_1	0.219		A_2	−0.984		A_2	−0.142
	E	−0.069	9_9	A_2	0.966		$F_2^{(1)}$	−1.956
	F_2	−0.136		$F_2^{(2)}$	0.861		$F_1^{(1)}$	−1.962
	A_2	−0.233		$F_1^{(3)}$	0.765	12_{12}	A_2	1.533
5_5	$F_1^{(2)}$	0.306		A_1	0.335		A_1	1.279
	E	0.247		$F_1^{(2)}$	0.073		$F_2^{(3)}$	1.438
	F_2	−0.221		E	0.056		$F_1^{(3)}$	1.326
	$F_1^{(1)}$	−0.322		$F_2^{(1)}$	−1.254		$E^{(2)}$	0.740
6_6	A_2	0.499		$F_1^{(1)}$	−1.269		$F_1^{(2)}$	0.748
	F_2	0.379	10_{10}	$E^{(2)}$	1.011		$F_2^{(2)}$	−0.198
	$F_1^{(2)}$	0.262		$F_1^{(3)}$	1.001		$F_1^{(1)}$	−0.253
	A_1	−0.378		$F_2^{(2)}$	0.842		$F_2^{(1)}$	−2.345
	$F_1^{(1)}$	−0.464		A_2	0.602		A_2	−2.378
	E	−0.491		$F_2^{(1)}$	0.099		$E^{(1)}$	−2.344
7_7	$F_1^{(2)}$	0.594		$F_1^{(2)}$	0.081			
	E	0.399		A_1	−1.388			
	$F_2^{(2)}$	0.298		$E^{(1)}$	−1.532			
	A_2	0.143		$F_1^{(1)}$	−1.610			
	$F_1^{(1)}$	−0.661						
	$F_2^{(1)}$	−0.666						

TABLE V

J_{J-1} LEVELS: SPLITTING PERTURBATIONS

1_0	A_1	0	8_7	$F_1^{(1)}$	0.083 cm^{-1}	11_{10}	$F_2^{(1)}$	−0.111 cm^{-1}
2_1	F_2	0		$F_2^{(1)}$	0.064		A_2	−0.112
3_2	E	0.006 cm^{-1}		A_1	−0.129		$E^{(1)}$	−0.128
	F_2	−0.008		$F_1^{(2)}$	−0.159		$F_1^{(1)}$	−0.288
4_3	F_2	0.016		E	−0.185		$F_2^{(2)}$	−0.375
	F_1	−0.012		$F_2^{(2)}$	−0.199		$E^{(2)}$	−0.379
	A_1	−0.051	9_8	$F_1^{(1)}$	0.049 cm^{-1}		A_1	−0.445
5_4	A_1	0.046		$E^{(1)}$	0.035		$F_1^{(2)}$	−0.422
	F_1	0.010		A_1	0.005		$F_2^{(3)}$	−0.400
	E	−0.012		$F_2^{(1)}$	−0.194	12_{11}	$F_2^{(1)}$	−0.223
	F_2	−0.075		$F_1^{(2)}$	−0.227		$F_1^{(1)}$	−0.243
6_5	$F_2^{(1)}$	0.046		$E^{(2)}$	−0.270		$E^{(1)}$	−0.335
	F_1	0.000		$F_2^{(2)}$	−0.267		$F_1^{(2)}$	−0.337
	E	−0.098	10_9	$F_1^{(1)}$	−0.025		$F_2^{(2)}$	−0.468
	$F_2^{(2)}$	−0.112		$F_2^{(1)}$	−0.042		A_1	−0.489
7_6	E	0.044		$F_2^{(2)}$	−0.262		$E^{(2)}$	−0.548
	$F_2^{(1)}$	0.030		A_2	−0.236		$F_1^{(3)}$	−0.551
	A_2	−0.002		$F_2^{(3)}$	−0.305		$F_2^{(3)}$	−0.586
	$F_2^{(2)}$	−0.121		$F_1^{(2)}$	−0.316			
	F_1	−0.149		E	−0.405			
	A_1	−0.171		A_1	−0.330			

TABLE VI

COMPARISON BETWEEN THEORY AND EXPERIMENT: P BRANCH

Observed frequencies[a]		Corrected for splitting perturbation
P(1)	cm^{-1}	cm^{-1}
F_2	3009.000	3009.00
P(2)		
E	2999.057	2999.02
F_2	.000	.02
P(3)		
F_2	2989.045	2988.97
F_1	2988.945	.92
A_1	.800	.94
		Ave. 2988.94$_6$
P(4)		
A_1	2979.033	2978.85
F_1	2978.937	.84
E	.872	.84
F_2	.656	.81
		Ave. 2978.83$_8$
P(5)		
F_2	2968.861	2968.63
F_1	.748	.63
E	.456	.59
F_2	.404	.61
		Ave. 2968.61$_4$
P(6)		
E, F_2[b]	2958.636	2958.34
A_2	.508	.33
F_2	.210	.32
F_1	.109	.32
A_1	.009	.32
		Ave. 2958.32$_8$
P(7)		
F_2	2948.465	2948.04
F_1	.405	.03
A_1	.081	.00
F_1	2947.888	.00
E	.792	.00
F_2	.660	.00
		Ave. 2948.01$_1$
P(8)		
A_1	2938.222	2937.64
F_1, E	.168	.63
F_2	2937.736	.62
F_1	.456	.65
P(8) (cont'd.)	cm^{-1}	cm^{-1}
E	.260	.59
F_2	.208	.61
		Ave. 2937.62$_6$
P(9)		
F_2	2927.932	2927.20
F_1	.903	.22
E	.378	.17
F_2	.342	.19
A_2	.025	.18
F_2	2926.837	.21
F_1	.750	.18
A_2	.670	.18
		Ave. 2927.19$_2$
P(10)		
E, F_2, A_2	2917.610	2916.74
F_2	.032	.71
F_1	2916.938	.71
A_1	.730	.71
F_1	.373	.72
E	.293	.73
F_2	.183	.72
		Ave. 2916.72$_4$
P(11)		
F_2, F_1	2907.285	2906.21
F_1	2906.688	.28
E	.592	.22
A_1	.560	.24
F_2	.232	.15
F_1	2905.770	.17
E	.647	.19
F_2	.507	.12
		Ave. 2906.20$_0$
P(12)		
A_1, F_1, E	2896.932	2895.67
F_2	.253	.58
F_1	.157	.63
E	2895.765	.56
F_2	.705	.55
A_2	.187	.67
F_2	.078	.65
F_1	.000	.61
A_1	2894.960	.62
		Ave. 2895.62$_6$

[a] Reference *3*.

[b] Lines such as these are unresolved.

TABLE VI—*Continued*

Observed Frequencies[a]		Corrected for splitting perturbation	Observed frequencies[a]		Corrected for splitting perturbation
P(13)			P(13) (cont'd.)		
F_2 , F_1	2886.570	2885.11	F_1	2885.190	2884.93
E	2885.823	4.96	A_1	2884.867	4.98
F_2	.803	4.99	F_1	.463	5.06
A_2	.718	5.06	F_2	.413	5.09
F_2	.310	4.96	E	.348	5.06
					Ave. 2885.02_6

is shifted to higher frequency by $[0.531-(-0.053)]$ cm^{-1} by the splitting perturbations of the excited and ground state, respectively, (Tables III and II). To obtain the unperturbed frequency of the second column of Table VI the perturbation of 0.584 cm^{-1} is subtracted from the observed frequency. If the theoretically predicted splitting perturbations are correct all the tetrahedral fine structure components of a given P line should coalesce to a single unperturbed frequency. From Table VI it is seen that the deviation from the average value of the unperturbed frequencies is generally within 0.02 cm^{-1} up to the tenth angular momentum quantum number but becomes as large as 0.09 cm^{-1} for $P(13)$. Table VII shows the comparison between theory and experiment for the R-branch lines in a similar way. If the splitting perturbations are handled in this way the analysis of the unperturbed P- and R-branch frequencies leads to rotational constants which can be compared with the theoretical expressions which were tabulated in (*1*). The results of the analysis give

$$\begin{aligned}(B_3 - B_0) &= -0.038_6 \text{ cm}^{-1},\\ 2(B_3 + B_0 - 2B_3\zeta_3) &= 19.745 \text{ cm}^{-1}.\end{aligned} \tag{3}$$

A theoretical D_s-value of 1.0×10^{-4} cm^{-1} has been used

$$D_s = 4B^3\left[\frac{2}{3\omega_1^2} + \frac{2}{15\omega_2^2} + \frac{\zeta_{23}^2}{5\omega_3^2} + \frac{\zeta_{24}^2}{5\omega_4^2}\right]. \tag{4}$$

The Q-branch lines show the largest splitting. The theoretically predicted Q branch is shown below the observed spectrum of Plyler *et al.* (*3*) in Fig. 1. The comparison between the observed and predicted Q-branch frequencies is also shown in Table VIII. The predicted frequencies are computed from the splitting perturbations of Tables II and IV and unperturbed Q-branch frequencies given by the following formula

$$Q(J) = \nu_0 - .0485\ J(J+1) + 4.5 \times 10^{-5}J^2(J+1)^2 \text{ cm}^{-1}, \tag{5}$$

where $Q(J) = \nu_0 + (B_3 - B_0)J(J+1)$ + fourth-order terms. Theory predicts that the effective B-value of the Q-branch should differ from that of the P and R

TABLE VII

COMPARISON BETWEEN THEORY AND EXPERIMENT. R BRANCH

Observed Frequencies[a]		Corrected for splitting perturbation	Observed frequencies[a]		Corrected for splitting perturbation
R(0)	cm^{-1}	cm^{-1}	R(8)	cm^{-1}	cm^{-1}
A_1	3028.744	3028.74_4	F_1, E, A_1	3104.598	3104.52
R(1)			F_2	.374	.57
F_2	3038.498	3038.49_8	F_1	.309	.56
R(2)			E, F_2	.248	.56
E, F_2[b]	3048.180	3048.18_2			Ave. 3104.54_6
R(3)			R(9)		
F_2, F_1[b]	3057.739	3057.74	F_2, F_1	3113.720	3113.67
A_1	.692	.74	F_2	.423	.69
		Ave. 3057.74_0	A_2	.403	.67
R(4)			F_2, F_1, E, A_1	.300	.69
A_1, F_1, E	3067.266	3067.24			Ave. 3113.68_3
F_2	.167	.24	R(10)		
		Ave. 3067.24_1	F_2, A_2, E	3122.775	3122.76
R(5)			F_1	.435	.73
F_2	3076.738	3076.68	F_2	.382	.75
F_1	.696	.69	E, A_1, F_1, F_2	.272	.77
E, F_2	.576	.69			Ave. 3122.75_8
		Ave. 3076.68_9	R(11)		
R(6)			F_1, F_2	3131.749	3131.79
E, F_2	3086.070	3086.02	F_1, E	.529	.85
A_2	.046	.04	A_1, F_2	.382	.90
F_2, F_1, A_1	.862	.03	F_1, E	.259	.94
		Ave. 3086.02_7	F_2	.197	.93
R(7)					Ave. 3131.87_5
F_1, F_2	3095.368	3095.27			
A_1, F_1	.174	.32			
E, F_2	.110	.33			
		Ave. 3095.30_5			

[a] Reference *3*.

[b] Lines such as these are unresolved.

branch (*1*). From Eqs. (3) and (5) it is seen that the difference is about 0.01 cm^{-1}. For low values of J the predicted Q-branch lines lie almost without exception within 0.02 cm^{-1} of the observed lines. For values of $J > 9$ the differences become somewhat larger, partly because the J-dependence of the centers of gravity of the Q-branch lines is no longer given very accurately by Eq. (5).

FORBIDDEN LINES

If matrix elements off-diagonal in the rotational angular momentum quantum number, R, give significant contributions to the energies of the vibration-rota-

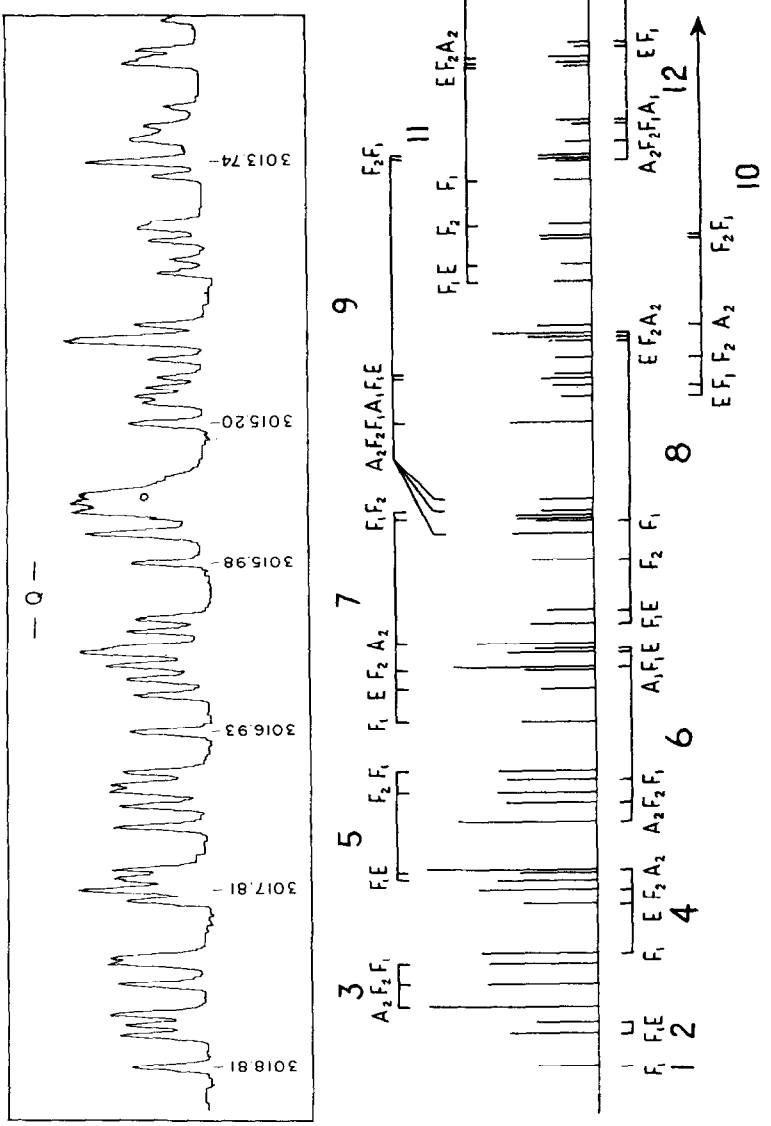

FIG. 1. Q branch. Comparison between theory and experiment

TABLE VIII

Q-BRANCH FREQUENCIES. COMPARISON BETWEEN THEORY AND EXPERIMENT

Line	Observed[a]	Predicted[b]	Line	Observed	Predicted
$1F_1$	3018.81 cm^{-1}	(3018.81) cm^{-1}	$7F_1^{(2)}$	3016.93 cm^{-1}	3016.90 cm^{-1}
$2F_1$	.65	.65	$7E$	.73	.72
$2E$	.60	.59	$7F_2^{(2)}$	.64	.62
$3A_2$	.53	.51	$6A_1$	.57	.58
$3F_2$	.35	.35	$6F_1^{(1)}$		.50
$3F_1$	.23	.25	$6E$	.48	.48
$4F_1$	.21	.18	$7A_2$		.48
$4E$	3017.87	.89	$8F_1^{(2)}$	.38	.36
$4F_2$	.82	.83	$8E^{(2)}$	.30	.27
$5F_1^{(2)}$		.79	$8F_2^{(2)}$	3015.98	3015.97
$5E$	.75	.74	$9A_2$	.79	.80
$4A_2$	.71	.73	$8F_1^{(1)}$		.72
$6A_2$	.45	.44	$7F_1^{(1)}$	.66	.70
$6F_2$	.32	.32	$7F_2^{(1)}$	H_2O	.70
$5F_2$	.25	.27	$9F_2^{(2)}$		.70
$6F_1^{(2)}$		.21	$9F_1^{(3)}$	.55	.62
$5F_1^{(1)}$	.17	.17	$9A_1$	.21	.21

[a] Reference *3*.

[b] From Eq. (5) and Tables II and IV.

tion levels, they may also be responsible for the appearance of weak infrared absorption lines in the P^0, P^-, R^+, R^0, Q^+, and Q^- branches which are forbidden in first approximation. The selection rule $\Delta R = 0$, valid for the fundamental, restricts the infrared active transitions to those of the P^+ branch, (transitions from the ground-state levels $(J + 1)$ to the excited state levels J_{J+1}), the Q^0 branch, (transitions from J to J_J), and the R^- branch, (transitions from $(J - 1)$, to J_{J-1}). If matrix elements off-diagonal in R give significant contributions to the energies, however, the true wave function of a state J_R is a linear combination of the zeroth-order wave functions of all three states J_{J+1}, J_J, and J_{J-1}. The fact that the rotational angular momentum quantum number, R, is not rigorously a "good quantum number" becomes important. Even if the major contribution to the infrared intensities comes from the first derivative term in the electric dipole moment expansion and is governed by the selection rule $\Delta R = 0$ involving the *zeroth-order* wave functions, lines in all three P, Q, and R branches become active since each state involves a mixture of all three possible values of the quantum number R.

The diagonalization process outlined above gives not only the corrected energies but also the correct linear combination of zeroth order wave functions. As a rule the amount of admixtures of states of different rotational angular momentum, R, are small but, especially in the case of large angular momenta, become significant enough to give rise to observable forbidden lines. Many weak lines

have been observed by Plyler and Allen (*3*, *5*) between the strong lines of the allowed P, Q, and R branches. Some of these must be attributed to the forbidden overtone $2\nu_2$ (activated through Coriolis interaction with $\nu_2 + \nu_4$ for example). Others still probably arise from hot bands; but many can be identified as the forbidden P-, Q-, and R-branch lines. In order to make the identification it is necessary to have an estimate of the relative intensities of the tetrahedral fine structure components of these lines. For the lines of the allowed P, Q, and R branches the transition probabilities are independent of K_R so that the relative intensities of the A, E, and F lines are governed solely by the statistical weight factors of 5, 2, and 3. The relative intensities of the A, E, and F lines of the forbidden branches, however, are determined by the degree of mixing of wave functions of different R. Since this is determined in a complicated way by the matrix elements off-diagonal in R, the relative intensities of the tetrahedral fine structure components vary from line to line in a nonsystematic way. With the somewhat drastic assumption that the intensities of the forbidden lines arise only from the first term in the electric dipole moment expansion the intensities of the forbidden lines can be computed from a knowledge of the correct linear combinations of zeroth-order wave functions.

Some characteristic examples of theoretically-predicted forbidden R-branch lines are shown in Figs. 2 and 3 below the spectra of Plyler *et al.* (*3*) run under conditions to bring out the weak lines. Although the predicted frequencies always lie within a few hundredths of a wave number of an observed weak line the agreement between the intensities of the theoretically-predicted and observed lines is at best qualitative. The number above the strongest line indicates the predicted intensity of the line relative to the intensity of an F line of the corresponding allowed R-branch transition. For example, the A_1 line of the branch $R^0(8 \rightarrow 9_9)$ should have an intensity 5×10^{-2} times the intensity of an F line of $R^-(8)$.

The predicted frequencies of the R^0 and R^+ lines follow from the observed frequencies of the allowed Q^0 and P^+ lines, respectively, and the energy differences between the $(J-1)$, J, and $(J+1)$ ground state levels. The following ground-state constants were used in computing the frequencies of the forbidden lines:

$$B_0 = 5.240\ \text{cm}^{-1}, \qquad D_s = 1.0 \times 10^{-4}\ \text{cm}^{-1}, \qquad D_t = 4.5 \times 10^{-6}\ \text{cm}^{-1}. \quad (6)$$

In principle the frequencies of the forbidden lines can be used to compute very accurate values for the ground-state constants. In practice, unfortunately, the identification of the forbidden lines of large angular momentum may be in some doubt since the predicted intensities may not be reliable and since the forbidden P-, Q-, and R-branch lines of ν_3 seem to be overlapped by many other weak lines not related to ν_3. The scalar and tensor D-values in particular may therefore require further adjustment even though the predicted forbidden P- and R-branch lines all lie within a few hundredths of a wave number of an observed weak line. In principle the D_t value can be determined directly from the differ-

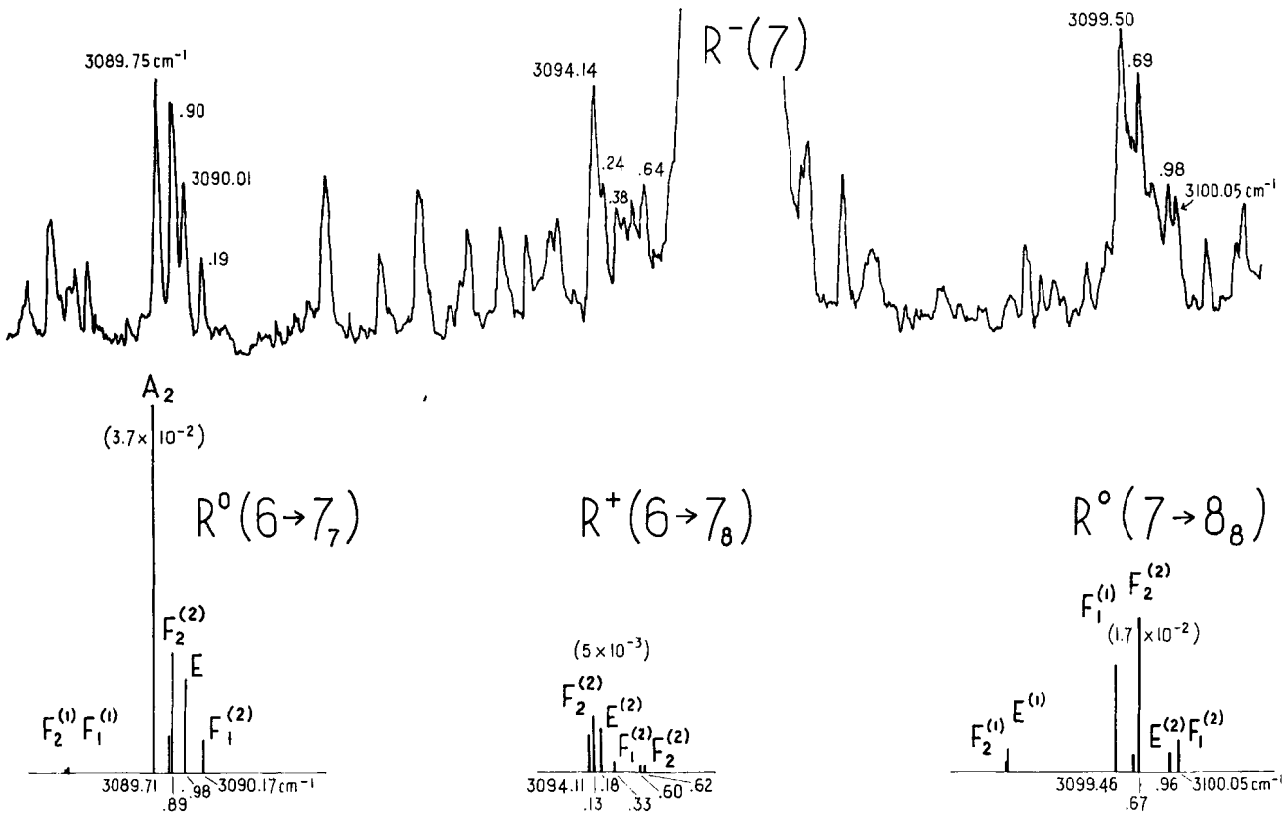

FIG. 2. Forbidden R-branch lines

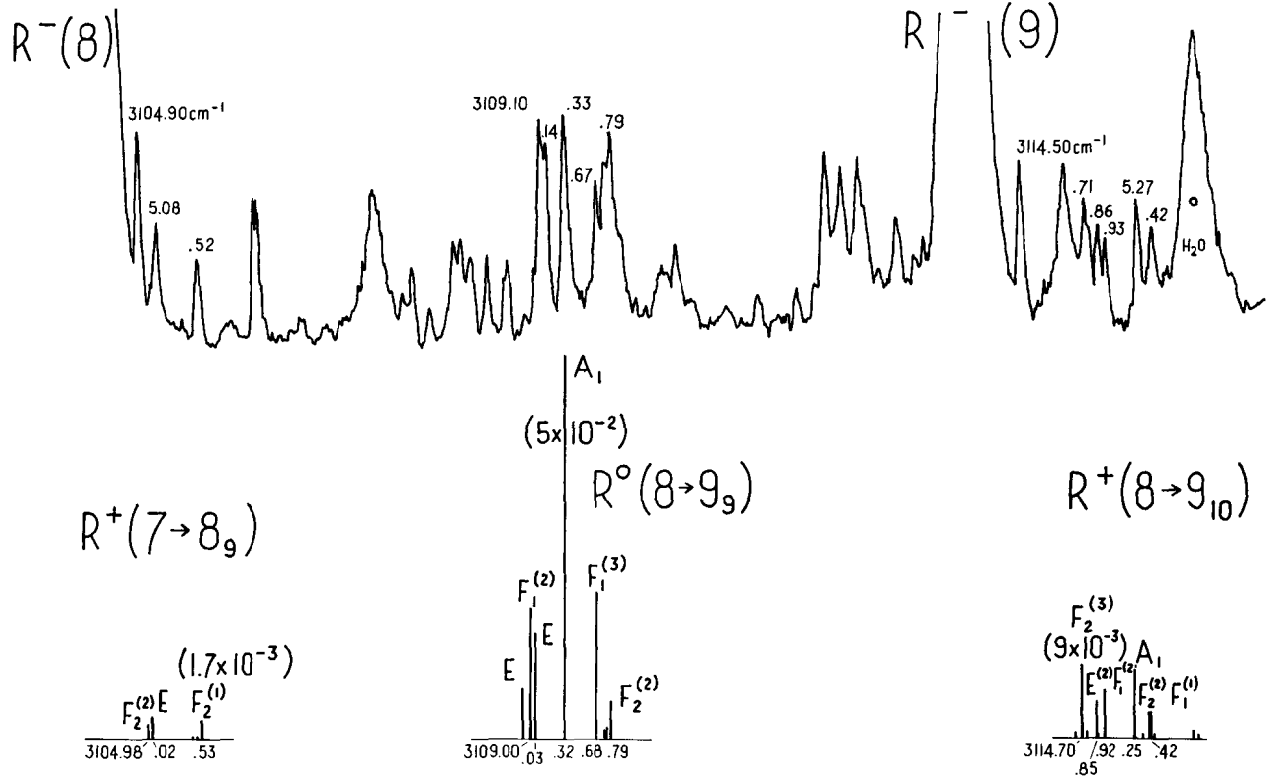

FIG. 3. Forbidden R-branch lines

ences of certain forbidden lines. In the case of the allowed P- and R-branch lines the selection rule $\Delta K_R = 0$ for the zeroth-order wave functions leads to the selection rule $F_2^{(1)} \rightarrow F_2^{(1)}$, $F_2^{(2)} \rightarrow F_2^{(2)}$, but $F_2^{(1)} \nrightarrow F_2^{(2)}$ if there are two F_2 substates for example. For the forbidden lines, however, the $F_2^{(1)} \rightarrow F_2^{(2)}$ and $F_2^{(2)} \rightarrow F_2^{(2)}$ transitions for example are both activated in the same order of approximation. The frequency difference between two such transitions is determined solely by the ground state D_t value. Unfortunately it was not possible to find two such lines of comparable intensity and sufficient frequency separation to be useful in determining D_t.

With the ground-state constants of Eq. (6) the constants for the fundamental ν_3 become

$$B_3 = 5.201\ \text{cm}^{-1}\ (R = \text{J} + 1, J - 1), \quad B_3 = 5.191\ \text{cm}^{-1}\ (R = J), \quad \zeta_3 = 0.054_7 .$$

ACKNOWLEDGMENT

I would like to thank Dr. E. K. Plyler of the National Bureau of Standards for making available prepublication copies of his spectra and for permission to reproduce the spectra of Figs. 1–3.

RECEIVED: June 28, 1960.

REFERENCES

1. K. T. HECHT, *J. Mol. Spectroscopy* **5,** 355 (1960). In this issue.
2. H. A. JAHN. *Proc. Roy. Soc.* **A168,** 469 and 495 (1938).
3. E. K. PLYLER, E. D. TIDWELL, AND L. R. BLAINE, *J. Research Natl. Bur.* **64A,** 201 (1960).
4. L. H. JONES AND R. S. MCDOWELL, *J. Mol. Spectroscopy* **3,** 632 (1959).
5. H. C. ALLEN AND E. K. PLYLER, *J. Chem. Phys.* **26,** 972 (1957).